



Oxide nanolayer formation on surface of modified blast furnace sludge particles during voltammetric cycling in alkaline media

V. Novák¹ · B. Kostura¹ · P. Raška¹ · K. Peterek Dědková² · R.G. Mendes³ · T. Gemming³ · J. Leško¹

Received: 18 June 2020 / Revised: 31 August 2020 / Accepted: 4 September 2020 / Published online: 10 September 2020
© Springer-Verlag GmbH Germany, part of Springer Nature 2020

Abstract

Knowledge of the properties of metallurgical waste is essential for the assessment of their recycling. In this work, the formation of iron oxide nanolayers during voltammetric cycling in 1 M NaOH on the particle surface of blast furnace sludge after acid leaching (BFSL) was studied. Most importantly, the effect of hydrogen on these processes was of particular interest. For these purposes, the study combines electrochemical methods, cyclic voltammetry on solid and carbon paste electrodes, with analytical optical methods (TEM). On the solid iron electrode surface as a model system, nanostructured magnetite (Fe₃O₄) was identified as the main oxidation product, and, to a lesser extent, also maghemite (γ-Fe₂O₃). It was found that the charges corresponding to Fe₃O₄ formation and its reduction together with the hydrogen evolution reaction (HER) occurring at $E = -1500$ mV depend on the number of cycles and have a similar course. Additionally, in the first phase of the cycling, the accumulation of maghemite on the solid Fe-electrode surface during cycling affects the growth of the oxide layer and catalytically increases the yield of the HER. Concerning the measurement with BFSL-modified CPE, on the BFSL surface, haematite is transformed into magnetite during cycling, resulting in the same Fe₃O₄ nanolayer as on the solid iron electrode. In this layer, the same redox processes take place, including the influence of hydrogen in the initial stage of cycling.

Keywords Iron electrode · Leached blast furnace sludge · Modified carbon paste electrode · Iron oxide nanolayer · Hydrogen evolution reaction

Introduction

Blast furnace sludge (BFS) is among the waste materials known to contain a relatively high content of heavy metals, especially zinc, cadmium, and lead, causing a significant environmental burden. Recycling focuses primarily on zinc separation by hydrometallurgical methods using different extraction agents [1, 2], most often inorganic or organic acids [3–5]. The blast furnace sludge after acid leaching (BFSL) partially

returns to the blast furnace cycle, but the rest remains unused and is landfilled. Electrochemical methods could be used for further processing. Detailed information on the electrochemical behaviour of this material is a key prerequisite for the achievement of success. Of interest is the alkaline environment in which iron and its oxides, the main components of BFS, are stable.

A Fe/alkaline system medium (1 M NaOH, KOH) stabilising electrochemical products on the iron electrode is usually used. In such an environment, Volpi found the coexistence of two main processes during cycling, one leading to Fe(OH)₂ and the other (reversible) to Fe^{III} oxo-compounds [6]. These reactions are essential for the oxide layer growth, significantly affecting the electrochemical response by hindering the charge transfer mechanism. As the thickness of the oxide layer increases, the charge transfer hinders, which in turn leads to a lower current response during anodic polarisation at different passivation times.

Cyclic voltammetry (CV) was supported by in situ Raman spectroscopy to describe electrochemical reactions [7–10]. Hugot [7] determined that the magnetite is formed in a wide

✉ B. Kostura
bruno.kostura@vsb.cz

¹ Department of Chemistry, VŠB - Technical University of Ostrava, 17. listopadu 2172/15, 708 00 Ostrava-Poruba, Czech Republic

² Centre for Advanced Innovation Technologies, VŠB-Technical University of Ostrava, 17. listopadu 2172/15, 708 00 Ostrava-Poruba, Czech Republic

³ Leibniz Institute for Solid State and Materials Research Dresden, Helmholtzstraße 20, 01069 Dresden, Germany

potential window and is the main component of the passive film. Moreover, Joiret [8] investigated electrochemical processes regarding the iron electrode at a low scan rate of 0.5 mV s^{-1} , also using electrochemical impedance spectroscopy and electrochemical quartz crystal microbalance. They observed that the passive film is based on magnetite and can be reduced or oxidised depending on the electrode potential. The presence of magnetite was confirmed in all potential ranges during forward (anodic) and reverse (cathodic) sweeps. The occurrence of magnetite as the only phase presented in the reverse scan at $E = -0.93 \text{ V}$ has not yet been clearly explained. Through micro Raman spectroscopy [9, 10], both the growth and composition of the passive film on iron were investigated at various stages by CV in 0.05 M NaOH .

Flis-Kabulska [11] studied hydrogen entry into iron from NaOH solutions during voltammetric cycling. The authors attempted to find a correlation between the hydrogen permeation maxima and the formation of surface films. Throughout the hydrogen evolution reaction (HER), hydrogen can enter the metal matrix during metal pickling in acids for scale removal, corrosion, and cathodic protection. The matter of hydrogen evolution reactions during CV has been previously assessed in work [12], where the hydrogen evolution and oxidation/reduction peak currents were measured to follow the loss of metal or oxide. For the sake of completeness, the iron oxy-hydroxide electrode's electrocatalytic properties were also investigated to clarify the oxygen evolution reaction (OER) in 1 M NaOH [13].

For the study of electrochemical properties of fine-grained metallurgical wastes and pure iron oxides as model substances, modified carbon paste electrodes (CPEs) can be utilised. These electrodes are mainly used as sensors for the determination of organic and inorganic compounds due to their unique properties [14]. Besides that, they allow electrochemical characterisation of iron oxide modifiers often in acidic media. A CPE modified by Fe_2O_3 was applied to study the catalytic efficiency of haematite on HER in acid and neutral media [15]. Throughout the dissolution of magnetite used as a modifier of CPE in acidic media, a kind of “Russian doll” effect was observed; that is to say, a generalised curve binds the voltammograms recorded at a different scan rate. This curve is characterised by a particular value of an “effective” scan rate corresponding to the pH of the solution [16]. Furthermore, it is noteworthy that the dissolution of iron(III) oxide-hydroxide is controlled by the surface reaction kinetics, and the position and shape of the voltammetric peaks can be used for the determination of oxide particle size [17, 18]. Mutombo confirmed the formation of higher nonstoichiometric iron oxide on the magnetite surface within passivation in acidic media [19].

This work aims to study the electrochemical reactions taking place on the surface of BFSL during repeated voltammetric cycling in an alkaline medium using the solid Fe-electrode and the modified paste electrode. It extends the

previous work [20]. Recently, the mechanisms of oxide nanolayer formation on the surface of the sludge particle and the influence of hydrogen on these redox processes were evaluated. Also, a close correlation between the formation of the nanomagnetite surface layer and the HER course was sought.

Experimental

Electrochemical cell

A three-electrode arrangement was applied for the experiments. Iron rods (99.98% Fe, 1 mm diameter) and modified carbon paste electrodes were used as working electrodes.

First, the Fe-electrode was cleaned chemically using concentrated HCl and then cathodically at $E = -1500 \text{ mV}$ for 5 min to remove air-formed oxides. After that, the electrode was immersed in acetone (Penta, ČR) to degrease its surface.

All potentials were referred to the SCE (saturated calomel electrode, 2THETA, CR). The counter electrode was a platinum wire with a large surface. The graphite powder (product CR 5 with average particle size $5 \mu\text{m}$, Maziva Tyn nad Vltavou, CR) and highly pure paraffin oil (Fluka) serving as a non-electrolyte binder were used for the preparation of carbon paste electrodes. The modified paste had the following composition: 59% graphite powder (particle size $< 5 \mu\text{m}$, 95%, Sigma-Aldrich), 26% spectroscopic pure paraffin oil and 15% of the modifier. Nanomagnetite, haematite and blast furnace sludge after acid leaching (BFSL) were used as modifiers. Prepared pastes were packed into a teflon holder of 2 mm inner diameter and then kept in a horizontal position for 24 h. Before each measurement, a new surface was obtained by ejecting approximately 1–2 mm of paste and thorough smoothing using a filter paper. All electrochemical measurements were performed in 1 M NaOH (Lachner) solution. The solutions were purged by nitrogen gas (Messer, CR) for 30 min before each experiment to maintain an inert atmosphere.

Leached blast furnace sludge

BFSL was obtained by leaching blast furnace sludge (North Moravian industrial agglomeration) for 48 h in 1 M HCl . The sludge granularity was modified by grinding and sieving below 0.18 mm . The detailed composition of BFSL is shown in Table 1. RTG analysis of BFSL showed that the main crystalline phase is haematite.

The elemental analysis was performed using the SPECTRO XEPOS energy dispersive X-ray fluorescence (XRF) spectrometer (Spectro Analytical Instruments, Germany). The determination of iron content was achieved using an AA280FS Atomic Absorption Spectrometer from Agilent Technologies.

Table 1 Elemental composition and crystalline phases of BFSL

Analyte	Fe _{total}	FeO	Si	Mg	Al	S	K	Ca	Cr	Mn	Zn	Ta	Pb
wt.%	47.00	4.64	3.20	0.35	0.96	0.37	0.12	0.27	0.03	0.09	0.05	0.01	< 0.001
Phase	Amorphous			Haematite			Magnetite		Quartz		Cristobalite		
wt.%	48.76			33.01			11.47		6.17		0.59		

Electrochemical instrumentation and settings

A Voltalab PGZ 301 potentiostat controlled by Voltmaster 4.0 software was used. All measurements were carried out by cyclic voltammetry (CV) at scan rate of $dE/dt = 100 \text{ mV s}^{-1}$.

RTG analysis

Powder X-ray diffraction analysis was carried out using a Bruker-AXS D8 Advance instrument with a $2\theta/\theta$ geometry measurement and the positionally sensitive detector LynxEye. The conditions were as follows: $\text{CoK}\alpha$ radiation Fe filter, 40 mA current, 40 kV voltage, step mode with a step of $0.014^\circ 2\theta$, and a total time of 25 s per step. The quantitative composition of the input sample (BFSL) was determined by the Rietveld method (Bruker TOPAS program) in combination with the internal standard method (ZnO, 10%).

TEM analysis

TEM experiments were carried out with using a TEM Tecnai F30 microscope (300 keV, field emission gun (FEG) cathode, spherical aberration coefficient $C_s = 1.2 \text{ mm}$) equipped with an energy dispersive X-ray spectrometer (EDXS) (Edax/Ametek TEAM Octane T Optima EDS windowless) and a multiscan CCD camera (Gatan MSC 794). Before the experiment, the iron electrode was immersed in deionised water and sonicated for 3 min, and a drop of the suspension was put on a mesh copper grid.

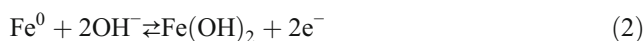
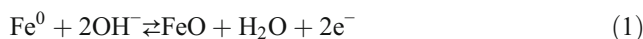
Results and discussion

Electrochemical reactions of solid Fe-electrode

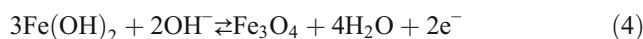
BFSL is a complex poly-component system containing mostly iron oxides (Table 1). For this material, the final reduction product is nanostructured Fe. Reaction processes taking place on the surface of the BFSL can be determined using the Fe-electrode owing to the similarity of both systems [20]. Since the electrochemical products under consideration are stable in alkaline media, the Fe/alkaline medium represents a pertinent model system for studying the mechanisms of oxide nanolayer formation.

Cyclic voltammetry (CV) was used to study the oxidation processes on the solid Fe-electrodes and the influence of hydrogen on them. In the potential window of -1500 – 500 mV at a scan rate of $dE/dt = 100 \text{ mV s}^{-1}$, one hundred cycles were measured (Fig. 1).

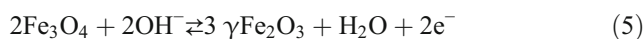
Two distinct peaks were recorded in both the anodic and cathodic regions (Fig. 1a). Peak I in the anodic region of CV at potential $E = -1090 \text{ mV}$ represents the oxidation of $\text{Fe}^0 \rightarrow \text{Fe}^{\text{II}}$, which can be expressed by Eqs. (1) and (2) [8, 21].



Peak II at potential $E = -690 \text{ mV}$ can be attributed to the oxidation of Fe^{II} to Fe^{III} , the formation of magnetite [8, 22], which can be described by Eqs. (3) and (4).



The gradual decrease near -500 mV suggests further oxidation processes, which are probably related to partial oxidation of magnetite to other forms of Fe^{III} according to Eqs. (5) and (6) [8]. The formation of metastable $\text{Fe}^{\text{II}}\text{-Fe}^{\text{III}}$ oxyhydroxides cannot be excluded either.



TEM was used to analyse the oxide layer formed on the solid Fe-electrode (Fig. 1b). It can be seen from the figure that the surface layer has visible crystal planes. According to the indexed planes, nanostructured magnetite is the primary oxidation product creating a porous layer on the electrode surface and, as a secondary product, maghemite ($\gamma\text{-Fe}_2\text{O}_3$) was identified.

In the reverse scan (Fig. 1a), two distinct peaks III and IV were observed, representing a complex transformation of $\text{Fe}^{\text{III}} \rightarrow \text{Fe}^{\text{II}} \rightarrow \text{Fe}^0$ (Eqs. 7–10) [23, 24]. At potentials close to $E = -1500 \text{ mV}$, hydrogen evolution occurs according to Eq. (11). On the surface of the solid iron electrode, hydrogen is present in the adsorbed form. It can also diffuse into the subsurface layer and weaken the metal bond, which can enhance the early stage of oxidation [25].

Fig. 1 Comparison of cyclic voltammograms of the iron electrode (a), onset potential –1500 mV, TEM analysis of oxidation product (b)

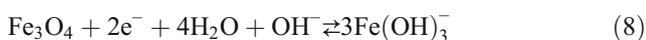
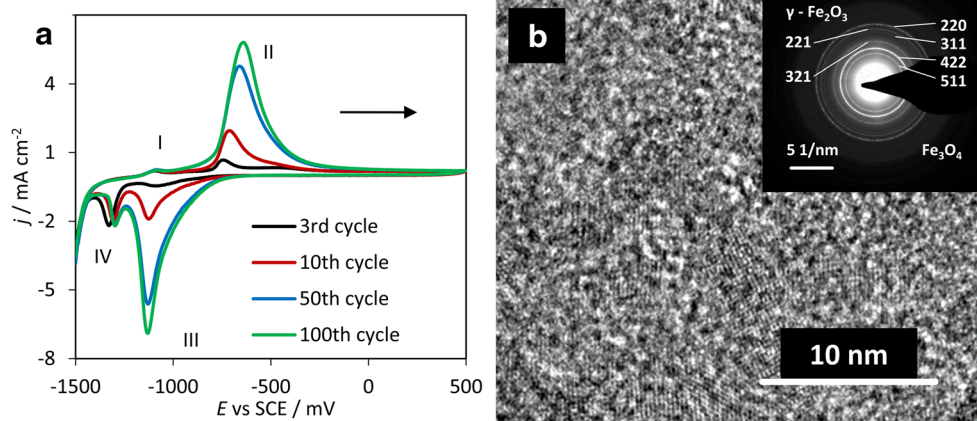


Figure 2 shows, in addition to the HER curve, the charges of peaks II and III during cycling, which are proportional to the mass of the magnetite produced by the oxidation (Eqs. 3 and 4) and its subsequent reduction in the reverse scan. The charges of peaks II and III were calculated according to Eq. (12)

$$Q = \int idt = \int C \frac{dE}{dt} dt = \int CdE \quad (12)$$

where Q is electric charge, C is capacitance and E is potential.

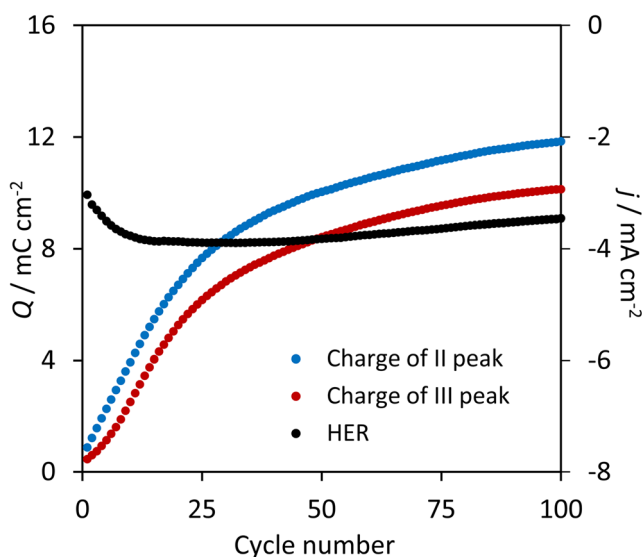


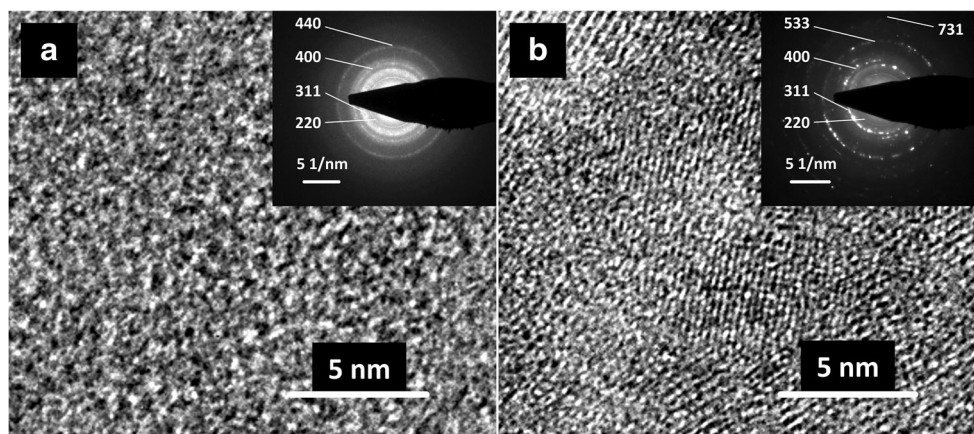
Fig. 2 The charges of particular peaks during cycling and course of HER at $E = -1500$ mV

The HER curve shows the magnitudes of the current responses at the potential $E = -1500$ mV. It was determined similarly as in the article [15]. In the first phase of layer growth, the charges of both peaks have an almost identical course and rise steeply up to approximately the 20th cycle. This phase can be interpreted following the article [26], where the accumulation of oxidation products on the iron surface and the continuous expansion of the oxide layer during cycling were found. After the first phase, the charge growth slows down and the oxide layer stabilises. These conclusions are consistent with the course of the HER curve, where initially, the amount of hydrogen increases, and then the equilibrium is established. The increase in hydrogen evolution in the first phase of cycling is probably influenced by the development of maghemite, which is electrochemically stable and catalyses hydrogen formation [27].

Furthermore, the charges corresponding to the formation of Fe_3O_4 and $\gamma\text{-Fe}_2\text{O}_3$ are higher than those of the opposite reduction process, implying that iron oxides are not entirely reduced and accumulation of oxides in the surface layer prevails during cycling [28]. According to indexed crystal planes, nanostructured magnetite remains the basis of the oxide layer formed at the end of the 10th and 50th cycle (Fig. 3a, b).

Significant differences in morphology and particle size depending on the voltammetric cycles indicate that during the first cycles, the growth of the nanomagnetite layer on the surface of the solid Fe-electrode is continuous (Fig. 3a). As cycling progresses, changes in the crystallinity take place (Fig. 3b). The diffractogram after the 50th cycle is not continuous due to considerable inhomogeneity of crystallite size. The formation of amorphous phases may be the cause. This finding confirms the assumption that the electrochemical processes are limited to the porous oxide layer formed on the metal surface during cycling. These results concur with the work [8], where Raman spectroscopy on a stationary Fe-electrode in 1 M NaOH unveiled the presence of magnetite in a reverse scan at a potential $E = -0.93$ V.

Fig. 3 TEM image of Fe-electrode after the 10th (a) and 50th (b) cycle, inlay denotes electron diffraction image



Electrochemical reactions of modified CPEs

The CPE was used to further study the effect of hydrogen on magnetite reduction and growth of the oxide layer throughout the cycling. To achieve that goal, the electrode was modified with nanostructured magnetite. Cyclic voltammograms were measured in different potential windows. In total, 100 cycles were performed in the potential range between $E = -1500$ mV and 500 mV. The applied scan rate was $dE/dt = 100$ mV s^{-1} . The results are summarised in Fig. 4.

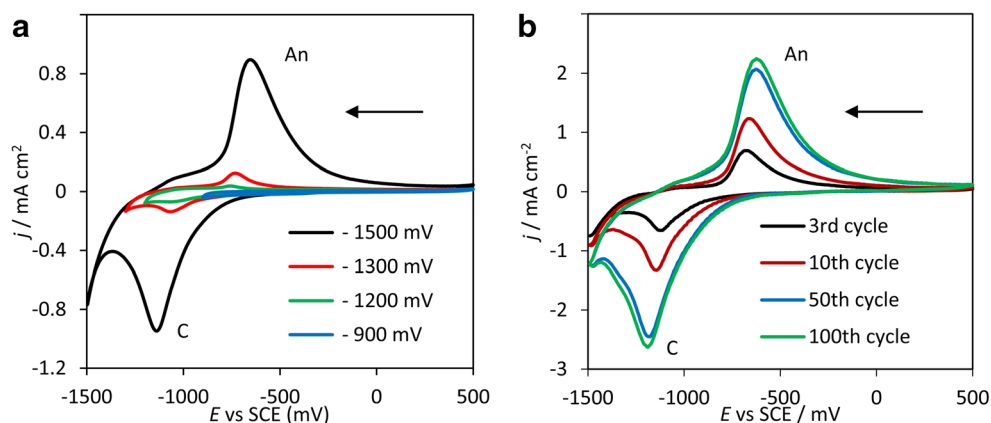
Figure 4a compares fifth cycles measured at different levels of cathodic polarisation. In comparison with the iron electrode, there was a merging of oxidation peaks into peak An and reduction peaks into peak C at the given scan rate. The figure shows a significant difference in cathodic and anodic peak currents depending on the ending potential applied. Up to a potential of -1200 mV, reduction and oxidation electrochemical processes are almost negligible.

As shown in Fig. 4b, the growth of peak currents An and C in the anodic and cathodic sweeps is most pronounced until the 50th cycle. During further cycling, the growth of both currents holds and the electrode reaches its equilibrium; i.e., voltammograms follow the same trend as with Fe-electrode (Fig. 1a).

According to Fig. 5, the charge changes and HER curve have the same course as in the case of the solid Fe-electrode (Fig. 2). On the surface of the original magnetite, a passive oxide layer forms and identical processes occur. As the particular charges are derived from the areas of oxidation and reduction peaks, their difference is related to the amount of non-reduced iron oxide and the formation of the oxide layer. Figures 2 and 5 show that the hydrogen evolution is closely related to the layer formation on both electrodes, the solid Fe-electrode and the modified CPE. Once the course of charge differences is constant, the hydrogen evolution stabilises. Its effect on redox processes is most significant at the initial stages of cycling. The mechanism of the HER in alkaline solutions involves adsorption of the hydrogen atom H_{ads} (Volmer reaction), desorption of hydrogen into solution (Heyrovsky reaction) and recombination of two hydrogen atoms to form a molecule of hydrogen gas (Tafel reaction). The combination of these processes is not excluded either. It has been found that the mechanism of the HER on a Fe_2O_3 - TiO_2 electrode in a 32% NaOH solution was controlled by a combination of Volmer-Heyrovsky reactions [29].

The aforementioned results were compared with CPE, where BFSL served as a modifier. The primary crystalline phase in BFSL was haematite (Fe_2O_3), as listed in Table 1.

Fig. 4 Voltammograms regarding carbon paste electrode modified with nanomagnetite, a comparison of fifth cycles at different levels of cathodic potential minima, b cycling up to 100th cycle, onset potential 500 mV, An and C denote anodic and cathodic peak, respectively



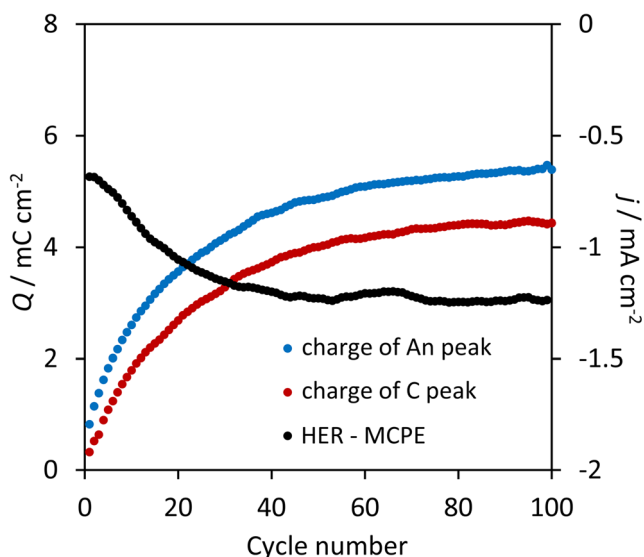


Fig. 5 Course comparison of charges corresponding to peaks An and C during cycling, HER curve for magnetite modified CPE

Figure 6 compares the cyclic voltammograms of CPE modified by BFSL. Recorded voltammograms were of a similar trend like those of a solid Fe-electrode and CPE modified by magnetite. Thus, it can be assumed that the identical processes befall on the BFSL surface during cycling.

Peaks I–II occur at the potentials similar to those regarding the Fe-electrode and represent the processes described by Eqs. 1–6. Reverse processes in the reduction region are represented by merged peak III. This peak represents a complicated reduction of Fe_2O_3 to Fe^0 , respecting the mechanism studied in [23, 29]. After the reaction of Fe_2O_3 with water, the formation of a complex $\text{Fe}(\text{OH})_4^-$ ion is assumed, which is gradually reduced

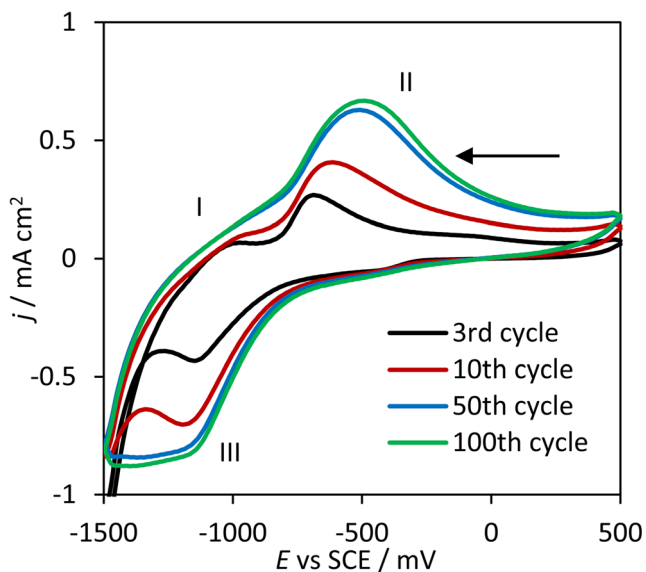


Fig. 6 Comparison of voltammograms of CPE modified by BFSL (1 M NaOH, $dE/dt = 100 \text{ mV s}^{-1}$), onset potential 500 mV

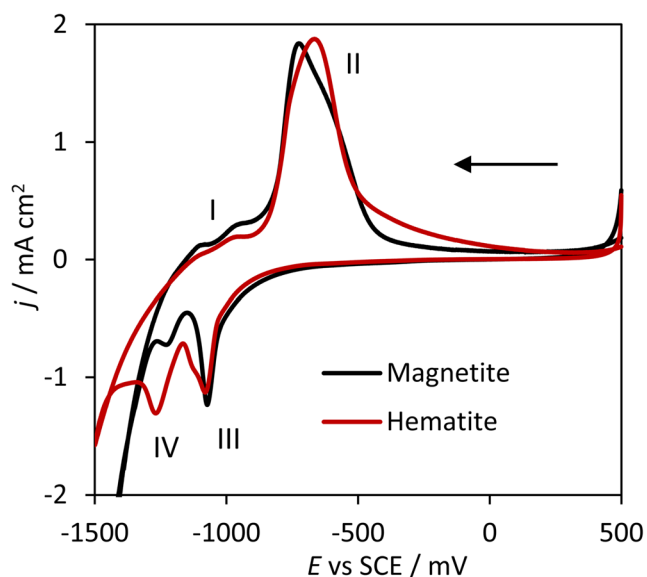


Fig. 7 Comparison of the 50th cycle of CPE modified by haematite and magnetite (1 M NaOH, $dE/dt = 2 \text{ mV s}^{-1}$), onset potential 500 mV

following the scheme $\text{Fe}(\text{OH})_4^- \rightarrow \text{Fe}(\text{OH})_3^- \rightarrow \text{Fe}^0$ [30]. In subsequent cycles, iron is oxidised to magnetite.

The transformation of haematite to magnetite is illustrated in Fig. 7, which compares the 50th cycles of CPE modified using haematite and magnetite. These electrodes were prepared with the same iron content in the paste. To explore cycling deeply, a lower scan rate was chosen.

The cyclic voltammograms of haematite and magnetite are almost identical (Fig. 7). Thus, magnetite nanolayers are formed on the surface of haematite and BFSL. The reduction of haematite to metallic Fe^0 is affected by hydrogen in the first phase of cycling, as shown in Fig. 8.

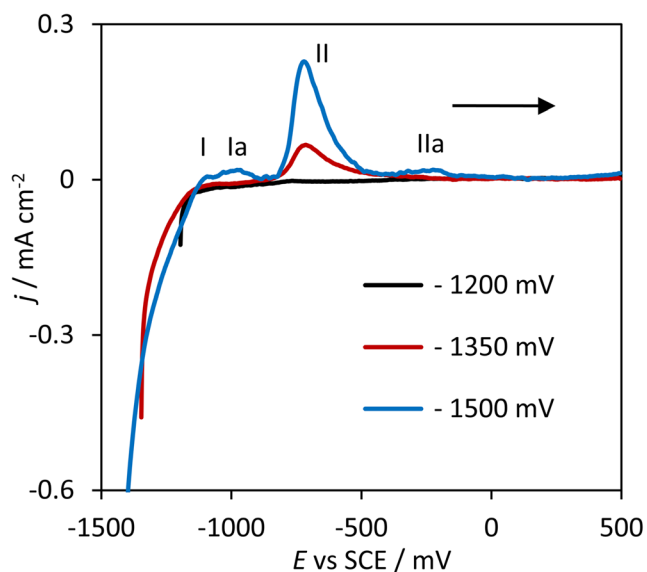


Fig. 8 Comparison of haematite anodic scans when cycling is initiated at different onset potentials (1 M NaOH, $dE/dt = 2 \text{ mV s}^{-1}$)

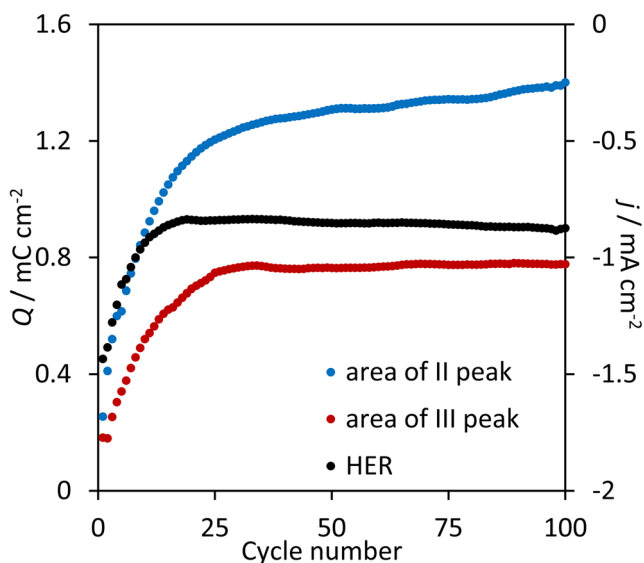


Fig. 9 Course comparison of charges corresponding to peaks II and III during cycling with HER curve for CPE modified by BFSL

This figure compares the forward scans of haematite when cycling is initiated at different potentials in the reduction region. The iron present in the haematite is in the maximum oxidation state. As expected, when the cycling starts at potentials higher than the hydrogen evolution potential, no oxidation processes occur. The formation of lower oxidation states occurs only at the potential of hydrogen evolution. These forms of iron are then gradually oxidised to magnetite in the anodic sweep. Gradual oxidation of Fe^0 to Fe^{II} corresponds to peaks I and Ia (Eqs. 1 and 2); peak II represents oxidation of Fe^{II} to magnetite (Eqs. 3 and 4). Peak IIa, a slight peak, indicates the formation of maghemite [8]. Its formation was proved by TEM analysis on the surface of the solid Fe-electrode in the anodic region (Fig. 1b).

Figure 9 shows that the charge changes as the function of the cycling of peaks II and III follow the same pattern as for the solid Fe-electrode (Fig. 2). The charges of both peaks rise steeply until about the 20th cycle, and then their growth slows down. The charges related to the formation of oxidation products are higher than those of the reduction process. It can be argued that formed magnetite is not entirely reduced and accumulates in the surface layer during cycling. From about the 20th cycle, the oxide layer stabilises. The HER curve shows the opposite course compared with the solid Fe-electrode. In the first stage of cycling, the amount of hydrogen decreases, and consequently, after the 20th cycle, equilibrium is established. It is clear that hydrogen also plays an essential role in the first phase of BFSL cycling. The opposite course of the HER curve can be explained by the fact that BFSL is a poly-component system containing not only iron oxides but also oxides of other metals, especially Mn and Zn.

Conclusion

Using the solid Fe-electrode as a model system, the characterisation of electrochemical processes taking place on the BFSL surface during cycling in an alkaline electrolyte was performed. TEM analysis revealed nanostructured Fe_3O_4 and $\gamma\text{-Fe}_2\text{O}_3$ at the end of the forward (anodic) scan and the presence of amorphous products at the end of the reverse (cathodic) scan. During voltammetric cycling, it was found that charges corresponding to the formation of Fe_3O_4 and $\gamma\text{-Fe}_2\text{O}_3$ and their reduction have a comparable course depending on the number of cycles. The difference of charges is related to the amount of unreduced iron oxide and the formation of a passive oxide layer and correlates with the course of the HER curves. The increase in current density of the HER can be explained by the presence of $\gamma\text{-Fe}_2\text{O}_3$, which is not directly reduced and catalyses hydrogen evolution in the initial cycling phase. Cyclic voltammetry on nanomagnetite modified carbon paste electrodes provided comparable results to the solid iron electrode. It has been found that identical processes also occur on the BFSL surface. During voltammetric cycling, haematite is transformed into magnetite. Hydrogen is also involved during the initial stages of this transformation. The formation of a magnetite layer on the BFSL surface involves the same mechanisms as the solid iron electrode. From the courses of HER curves, it is possible to determine when the oxide layer's thickness reaches its maximum. Electrochemically modified BFSL can be used as a sorbent to remove arsenic from wastewater, in electrical engineering for the manufacture of microchips and also as a material for electrochemical hydrogen production.

Funding This paper was created within the frame of the project number SP2019/142 financed by the Ministry of Education, Youth and Sports of the Czech Republic and the project number CZ.02.1.01/0.0/0.0/17_049/0008426 financed by Operational Programme Research, Development and Education under the auspices of the Ministry of Education, Youth and Sports of the Czech Republic.

Compliance with ethical standards

Competing interests The authors declare that they have no conflicts of interest.

References

1. Das B, Prakash S, Reddy PSR, Misra VN (2007) An overview of utilization of slag and sludge from steel industries. *Resour Conserv Recycl* 50(1):40–57
2. Huang X, Zhao H, Li X, Qiu W, Wu W (2007) Performance of planar SOFCs with doped strontium titanate as anode materials. *Fuel Cell Bull* 7:12–16
3. Langová Š, Leško J, Matýsek D (2009) Selective leaching of zinc from zinc ferrite with hydrochloric acid. *Hydrometallurgy* 95(3–4): 179–182

4. Asadi ZB, Mowla D, Shariat MH, Fathi KJ (1997) Zinc recovery from blast furnace flue dust. *Hydrometallurgy* 47(1):113–125
5. Steer JM, Griffiths AJ (2013) Investigation of carboxylic acids and non-aqueous solvents for the selective leaching of zinc from blast furnace dust slurry. *Hydrometallurgy* 140:34–41
6. Volpi E, Olietti A, Stefanoni M, Trasatti SP (2015) Electrochemical characterization of mild steel in alkaline solutions simulating concrete environment. *J Electroanal Chem* 736:38–46
7. Hugot-Le Goff A, Flis J, Boucherit N, Joiret S, Wilinski J (1990) Use of Raman spectroscopy and rotating split ring disk electrode for identification of surface layers on iron in 1M NaOH. *J Electrochem Soc* 137:2684–2690
8. Joiret S, Keddou M, Nóvoa X, Pérez M, Rangel C, Takenouti H (2002) Use of EIS, ring-disk electrode, EQCM and Raman spectroscopy to study the film of oxides formed on iron in 1M NaOH. *Cem Concr Compos* 24(1):7–15
9. Nieuwoudt MK, Comins JD, Cukrowski I (2011) The growth of the passive film on iron in 0.05 M NaOH studied in situ by Raman micro-spectroscopy and electrochemical polarisation. Part I: near-resonance enhancement of the Raman spectra of iron oxide and oxyhydroxide compounds. *J Raman Spectrosc* 42(6):1335–1339
10. Nieuwoudt MK, Comins JD, Cukrowski I (2011) The growth of the passive film on iron in 0.05 M NaOH studied in situ by Raman microspectroscopy and electrochemical polarization. Part II: in situ Raman spectra of the passive film surface during growth by electrochemical polarization. *J Raman Spectrosc* 42(6):1353–1365
11. Flis-Kabulska I, Zakroczyński T, Flis J (2007) Accelerated entry of hydrogen into iron from NaOH solutions at low cathodic and low anodic polarisations. *Electrochim Acta* 52(9):2966–2977
12. Song I, Gervasio D, Payer JH (1996) Electrochemical behaviour of iron and iron oxide thin films in alkaline (1 M KOH) aqueous solution: a voltammetry study for cathodic instability of coating/metal interface. *J Appl Electrochem* 26:1045–1052
13. Doyle RL, Lyons MEG (2013) An electrochemical impedance study of the oxygen evolution reaction at hydrous iron oxide in base. *Phys Chem Chem Phys* 15(14):5224–5237
14. Švancara I, Kalcher K, Walcarius A, Vytřas K (2012) *Electroanalysis with carbon paste electrodes*, 1st edn. CRC Press, Boca Raton
15. Akhtar A, Ghaffarnejad A, Hosseini SM, Manteghi F, Maminejad N (2015) Electrocatalytic hydrogen production by bulk and nano Fe₂O₃ and carbon nanotube modified with Fe₂O₃. *J Electroanal Chem* 739:73–83
16. Fetisov VB, Ermanov AN, Belysheva GM, Fetisov AV, Kamyshev VM, Brainina KZ (2004) Electrochemical dissolution of magnetite in acid solutions. *J Solid State Electrochem* 8:565–571
17. Grygar T (1997) Dissolution of pure and substituted goethites controlled by the surface reaction under conditions of abrasive stripping voltammetry. *J Solid State Electrochem* 1(1):77–82
18. Grygar T (1998) Phenomenological kinetics of irreversible electrochemical dissolution of meta-oxide microparticles. *J Solid State Electrochem* 2(3):127–136
19. Mutombo P, Hackerman N (1997) Potential decay behavior of iron in dilute nitric acid. *J Solid State Electrochem* 1(3):194–198
20. Novák V, Raška P, Matýšek D, Kostura B (2018) Electrochemical characterization of fine-grained blast furnace sludge after acid leaching using carbon paste electrode. *J Solid State Electr* 22(11):3457–3466
21. Liu M, Cheng X, Zhao G, Li X, Pan Y (2016) Corrosion resistances of passive films on low-Cr steel and carbon steel in simulated concrete pore solution. *Surf Interface Anal* 48(9):981–989
22. Freire L, Catarino MA, Godinho MI, Ferreira MJ, Ferreira MGS, Simoes AMP, Montemor MF (2012) Electrochemical and analytical investigation of passive films formed on stainless steels in alkaline media. *Cement Concrete Comp* 34(9):1075–1081
23. Allanore A, Lavelaine H, Valentin G, Birat JP, Delcroix P, Lapique F (2010) Observation and modeling of the reduction of hematite particles to metal in alkaline solution by electrolysis. *Electrochim Acta* 55(12):4007–4013
24. Monteiro JF, Ivanova YA, Kovalevsky AV, Ivanou DK, Frade JR (2016) Reduction of magnetite to metallic iron in strong alkaline medium. *Electrochim Acta* 193:284–292
25. Das NK, Shoji T (2013) An atomic study of hydrogen effect on the early stage oxidation of transition metal surfaces. *Int J Hydrogen Energ* 38(3):1644–1656
26. Schmuki P, Büchler M, Virtanen S, Isaacs HS, Ryan MP, Böhm H (1999) Passivity of Iron in alkaline solutions studied by in situ XANES and a laser reflection technique. *J Electrochem Soc* 146:2097–2102
27. Davodi F, Mühlhausen E, Tavakkoli M, Sainio J, Jiang H, Gökce B, Marzun G, Kallio T (2018) Catalyst support effect on the activity and durability of magnetic nanoparticles: toward design of advanced electrocatalyst for full water splitting. *ACS Appl Mater Interfaces* 10(37):31300–31311
28. Weinrich H, Gehring M, Tempel H, Kungl H, Eichel RA (2019) Electrode thickness-dependent formation of porous iron electrodes for secondary alkaline iron-air batteries. *Electrochim Acta* 314:61–71
29. Shibli SMA, Sebeelamol JN (2013) Development of Fe₂O₃-TiO₂ mixed oxide incorporated Ni-P coating for electrocatalytic hydrogen evolution reaction. *Int J Hydrog Energy* 38(5):2271–2282
30. Zou X, Gu S, Cheng H, Lu X, Zhou Z, Li C, Ding W (2015) Facile electrodeposition of iron films from NaFeO₂ and Fe₂O₃ in alkaline solutions. *J Electrochem Soc* 162(1):D49–D55

Publisher's note Springer Nature remains neutral with regard to jurisdictional claims in published maps and institutional affiliations.